ANL-HEP-PR-03-063, FERMILAB-Pub-03/234-T, DESY-03-036

November 13, 2003

Next-to-leading order QCD predictions for $W + 2$ jet and $Z + 2$ jet production at the CERN LHC

John Campbell*

HEP Division, Argonne National Laboratory,

9700 South Cass Avenue, Argonne, IL 60439

R. K. Ellis†

Theory Group, Fermi National Accelerator Laboratory,

P.O. Box 500, Batavia, IL 60510

D. Rainwater‡

Theory Group, DESY

Notkestrasse 85, Lab. 2a,

D-22603 Hamburg, Germany

Abstract

We present cross sections and differential distributions for QCD radiative corrections to the QCD processes $pp \to W + 2$ jets and $pp \to Z + 2$ jets at the CERN LHC. Calculations are performed with the Monte Carlo program MCFM. Cross section dependence on the renormalization and factorization scales is greatly reduced, except for the heavy-flavor case of $W^{\pm} b\bar{b}$, which has new features at next-to-leading order at the LHC. We also present cross sections for $W^{\pm} b\bar{b}$ and $Z+2$ jets in kinematic configurations relevant for Higgs boson searches.

PACS numbers: 13.38 -b, 12.38 -t

*Electronic address: johnmc@hep.anl.gov

†Electronic address: ellis@fnal.gov

‡Electronic address: david.rainwater@desy.de

I. INTRODUCTION

We report on the results of a calculation of the next-to-leading (NLO) order QCD corrections to the QCD processes

$$\begin{aligned} pp &\to W^{\pm} + 2 \text{ jets} \to \ell^{\pm}\nu + 2 \text{ jets} , \\ pp &\to Z/\gamma^* + 2 \text{ jets} \to \ell^+\ell^- + 2 \text{ jets} . \end{aligned} \tag{1}$$

(single flavor, $\ell = e, \mu$ or τ) at the CERN Large Hadron Collider (LHC), *i.e.* pp collisions at $\sqrt{s} = 14$ TeV. We ignore electroweak (EW) contributions arising from *e.g.* t-channel $W/Z/\gamma$ exchange between two scattered quarks, which are typically $\mathcal{O}(1\%)$ for total rates. Calculations for the Fermilab Tevatron, $p\bar{p}$ collisions at $\sqrt{s} = 2$ TeV, were considered in a previous publication [1], which also introduced the calculational technique. The results are made with the Monte Carlo program MCFM, which makes full predictions for any infra-red safe variable, including fully differential distributions, for any set of experimental cuts, and any decay modes of the Z/γ^* intermediate states. However, here we consider only leptonic vector boson decays. All leptons are treated as massless, so the results treat $W, Z \to e, \mu, \tau$ flavors as equivalent.

MCFM uses previously published matrix elements for the crossed reactions $e^+e^- \to$ 4 partons [2] and $e^+e^- \to 5$ partons [3], in the four dimensional helicity scheme. The real corrections to the basic Born processes, *i.e.*

$$\text{parton} + \text{parton} \to W/Z/\gamma^* + 3 \text{ partons} \tag{2}$$

were published in Refs. [3–5]. MCFM incorporates these matrix elements using the subtraction method [6, 7]. These details and those of the numerical checks performed may be found in Ref. [1].

As a useful comparison to more inclusive, well-studied weak boson production, we simultaneously present MCFM results for the processes $W, Z + 0,1$ jets. QCD corrections for these processes have been known for some time [8], and have already proved invaluable for Tevatron studies. The inclusion of the $W/Z + 1$ jet processes in MCFM aided in understanding the issues to be faced in implementing the more complicated $W/Z + 2$ jet processes. The next-to-next-to-leading order (NNLO) corrections to total inclusive W, Z production are known [9], but are not implemented in MCFM.

Parameter	Default value	Parameter	Default value
M_Z	91.187 GeV	$\alpha(M_Z)$	1/128.89
Γ_Z	2.49 GeV	G_F	1.16639×10^{-5}
M_W	80.41 GeV	g_w^2	0.42662 (calculated)
Γ_W	2.06 GeV	$\sin^2\theta_w$	0.23012 (calculated)

TABLE I: Default parameters in the program MCFM.

We also present results where the additional jets are a heavy flavor pair, specifically b quarks, *i.e.* $W^{\pm}b\bar{b}, Zb\bar{b}$, and compare to the flavor-inclusive expectations. This was previously studied for the Tevatron [10, 11], but our results are the first NLO predictions for these rates at the LHC. These are of particular importance as backgrounds to a number of new physics searches, especially for the Higgs boson. Experimental studies have so far had to rely on leading order (LO) predictions. For the $W^{\pm}b\bar{b}$ processes we find a LO calculation underestimates the rates at LHC energies by about a factor 2.4.

II. GENERAL RESULTS

Here we present results for the total observable cross sections for the production of a vector boson and up to 2 jets. Results specific to Higgs boson searches can be found in Section IV.

A. Input parameters

For all our results we use the default set of EW parameters in MCFM, which are given in Table I. As noted in the table, some parameters are calculated using the effective field theory approach [12],

$$e^2 = 4\pi\alpha(M_Z), \quad g_w^2 = 8M_W^2\frac{G_F}{\sqrt{2}}, \quad \sin^2\theta_w = \frac{e^2}{g_w^2}. \tag{3}$$

For simplicity we have taken the CKM matrix to be diagonal in the $W+2$ jets process. As a consequence there are, for example, no annihilating $u\bar{s}$ initial states for this case. This approximation is not expected to influence any anticipated analyses. For the other processes

we retain only the Cabibbo sector of the CKM matrix,

$$V_{CKM} = \begin{pmatrix} 0.975 & 0.222 & 0 \\ 0.222 & 0.975 & 0 \\ 0 & 0 & 1 \end{pmatrix} . \tag{4}$$

The value of $\alpha_S(M_Z)$ is not adjustable; it is determined by the chosen parton distribution. A collection of modern parton distribution functions (PDFs) is included with MCFM, but here we concentrate on the CTEQ6L1 (LO) and CTEQ6M (NLO) sets [13] which specify $\alpha_S(M_Z) = 0.130$ and $\alpha_S(M_Z) = 0.118$ respectively. Unless otherwise stated, we take the factorization and renormalization scales to be $\mu \equiv \mu_f = \mu_r = M_V$.

B. Basic kinematic cuts and jet selection

For the general results presented here, we consider single leptonic decays,

$$W^+ \to \nu e^+ , \qquad W^- \to \bar{\nu} e^- , \qquad Z/\gamma^* \to e^- e^+ . \tag{5}$$

W^+ and W^- must be considered separately for pp collisions, as their rates are not equal, given the unequal quark/anti-quark parton distributions.

Since these results are also intended to help calibrate experimentalists' Monte Carlo results, the results must be obtained with kinematic cuts on the final state particles for which they will be observable at the LHC experiments ATLAS and CMS. All leptons must satisfy

$$p_T(\ell) > 15 \text{ GeV}, \qquad |\eta_\ell| < 2.4, \tag{6}$$

We also require that the charged dilepton invariant mass be greater than 15 GeV. This prevents the production of soft $e^- e^+$ pairs which would otherwise be copiously produced by the virtual photon in the Z/γ^* process. We use the Run II k_T clustering algorithm [14] to find jets, with a pseudo-cone of size $R = 0.4$. Jets are also subject to kinematic cuts consistent with detector requirements for observability:

$$p_T(j) > 20 \text{ GeV}, \qquad |\eta_j| < 4.5. \tag{7}$$

Finally, we require a minimum separation to isolate the leptons:

$$\triangle R_{\ell j} > 0.4 \ , \ \triangle R_{\ell\ell} > 0.2 \ . \tag{8}$$

For the specific case of heavy-flavor jets, which are experimentally observed via vertex tagging, the pseudo-rapidity restriction is more severe:

$$|\eta_b| < 2.5 \ . \tag{9}$$

We do not impose a cut on missing transverse momentum, $\not{p}_T$, for the $W^{\pm}+$ jets cases. Not all analyses planned for the LHC use such a cut, or use different values for it, depending on what else is required in the event and machine luminosity. Instead, we show the differential distribution in this variable.

Except where noted, we consider only inclusive jets production: $W, Z + n$ jets refers to the cross section for production of W, Z and n or more jets.

C. Scale dependence

The principal motivation for performing a NLO calculation is to reduce the uncertainties in LO predictions. In particular, any perturbative prediction contains an unphysical dependence on renormalization and factorization scales μ_r, μ_f. The scale μ_f is introduced during the factorization of the calculation into a perturbative hard scattering part and non-perturbative PDFs. The latter are taken as input from data, with additional perturbative evolution. The factorization and renormalization scales are often chosen to be equal, $\mu \equiv \mu_r = \mu_f$, and we do this here. Strictly speaking, the two scales are unrelated and a calculation should be checked for independence of each scale individually. However, MCFM does not currently allow for this possibility for most processes.

The magnitude of cross sections and the shape of differential distributions can vary greatly between two different choices of scale. This is often interpreted as an inherent "theoretical uncertainty". Another strategy is to argue for a particular choice of scale, based on the physics of the process under consideration. Sometimes this gives results at LO that are close to the NLO results, but is not guaranteed.

A NLO calculation is an invaluable tool for investigating the issue of scale dependence. In a calculation performed through to order α_s^n, the residual scale dependence enters only at order α_s^{n+1}. As a result, one expects that NLO predictions are more stable under variations of the scale, μ. In addition, the NLO result may provide further evidence to support a particular scale choice that may have been deemed appropriate at leading order. In this

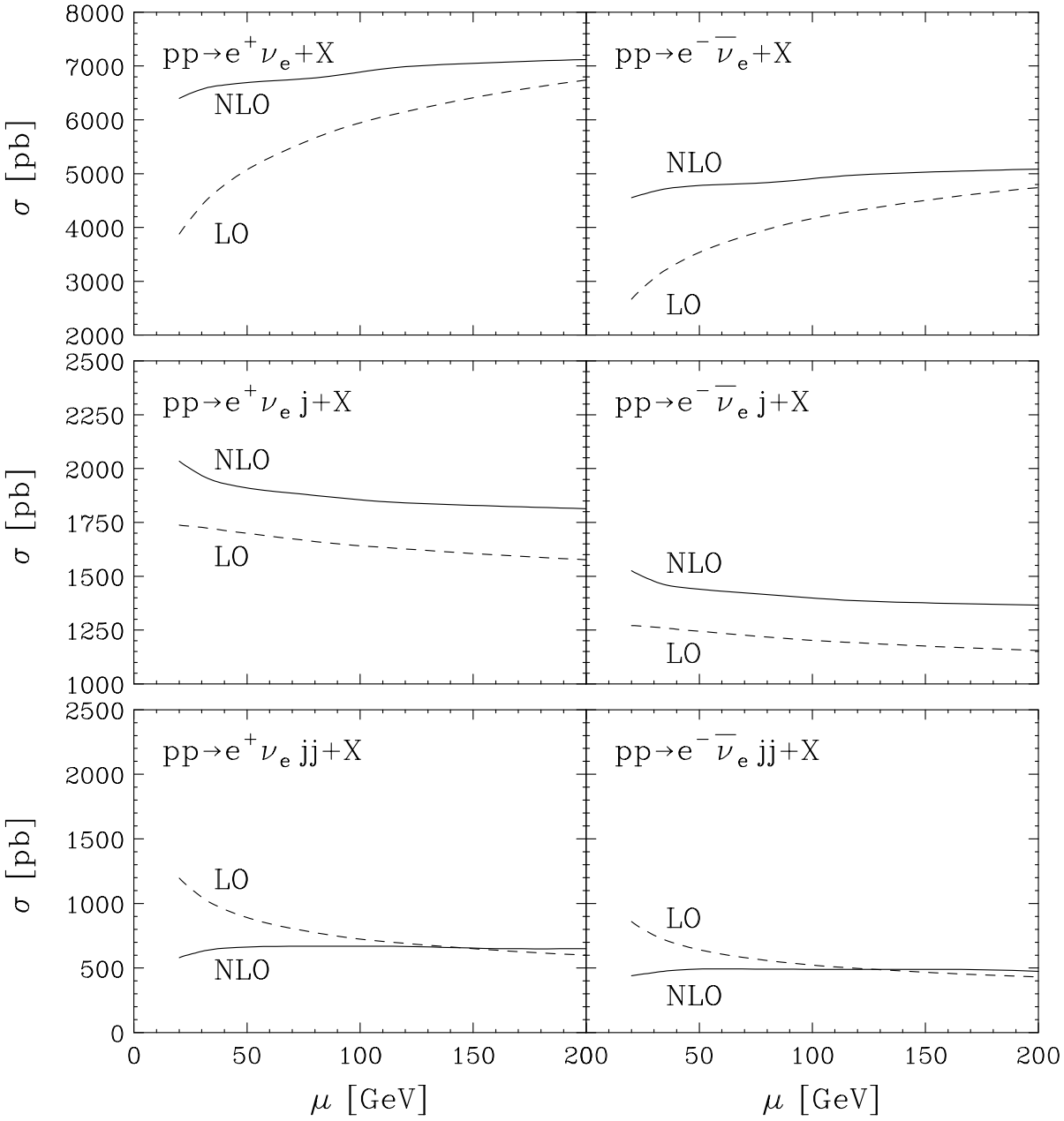

FIG. 1: Scale dependence of the $e\,\nu_e+$ jets cross sections, $\mu = \mu_r = \mu_f$, using the cuts described in Sec. II B. In general, μ-dependence is significantly reduced at NLO compared to LO.

case, the NLO result does not imply that the scale choice is physically meaningful, but it can provide an easy method of normalizing a LO calculation. (A LO calculation typically proceeds much more rapidly, and may need to be repeated multiple times for different kinematic configurations.)

To show the improvement achieved in the present calculation, we plot the scale dependence of the total inclusive $W, Z + 0, 1, 2$ jets cross sections, including leptonic decay, with

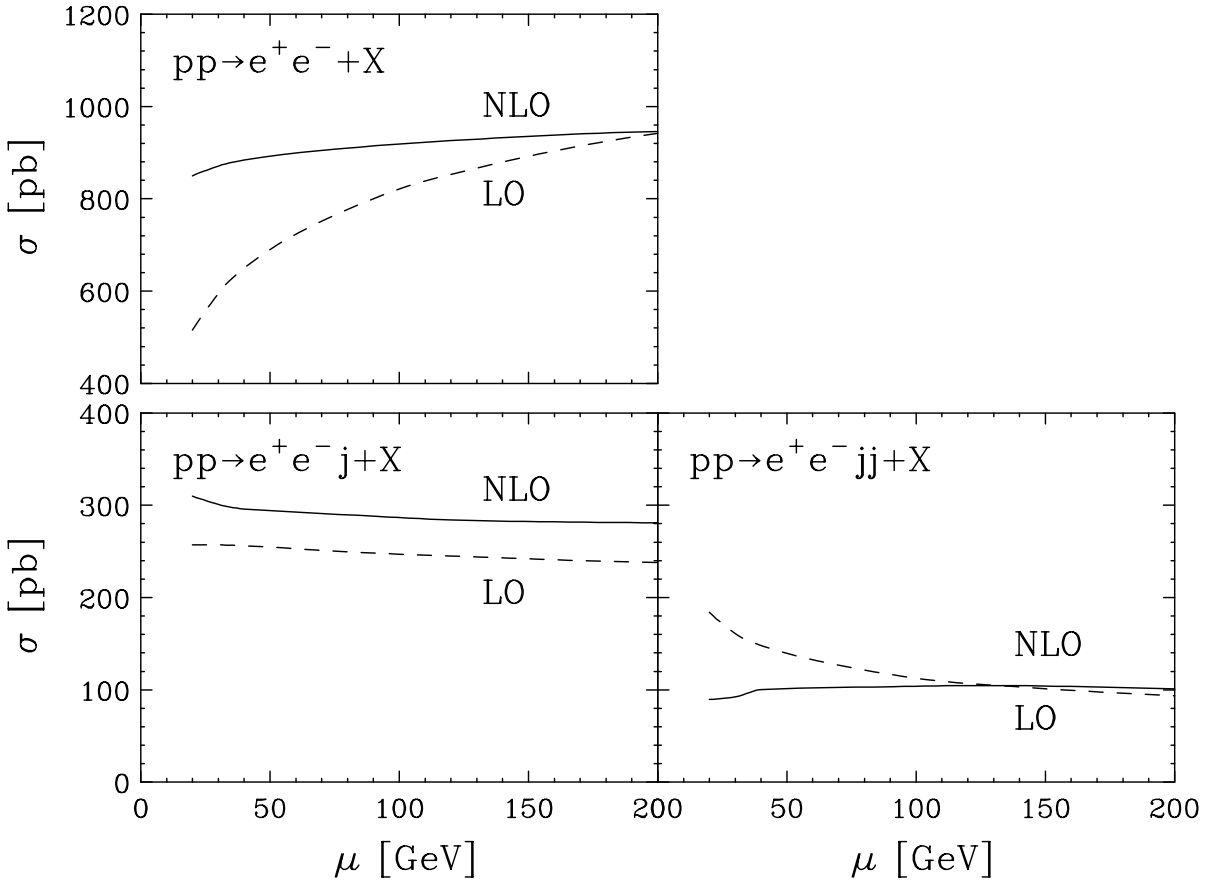

FIG. 2: Scale dependence of the e^+e^-j and e^+e^-jj cross sections, $\mu = \mu_r = \mu_f$, using the cuts described in Sec. II B.

the kinematic cuts of Eqs. (6-8), in Figs. 1,2. The NLO predictions for $W, Z + 0, 1$ jets have been known for some time [8, 15, 16], but we recalculate them here with MCFM. The $W + 2$ jets behavior, Fig. 1, is practically independent of μ, as in the $W, Z + 0, 1$ jets cases, demonstrating a small theoretical uncertainty. Table II summarizes the NLO results for $V+$ jets processes, along with the residual theoretical uncertainty due to scale dependence. All Monte Carlo statistical uncertainties are less than 1%. While the QCD corrections for $V + 0, 1$ jets are positive, for $V + 2$ jets they are slightly negative.

D. Kinematic distributions

Once again, we repeat some $W, Z + 1$ jet results, in order to highlight both the similarities and the differences with the corresponding 2-jet distributions. We first show the missing transverse momentum distributions for $W^{\pm}+$ jets in Fig. 3, and then the leading (hardest)

process	σ_{LO}	σ_{NLO}
$e^+\nu_e + X$	5670	6780^{+290}_{-130}
$e^-\bar{\nu}_e + X$	3970	4830^{+210}_{-90}
$e^+e^- + X$	803	915 ± 31
$e^+\nu_e\, j + X$	1660	1880^{+60}_{-50}
$e^-\bar{\nu}_e\, j + X$	1220	1420 ± 40
$e^+e^-\, j + X$	248	288^{+8}_{-7}
$e^+\nu_e\, jj + X$	773	669^{+0}_{-18}
$e^-\bar{\nu}_e\, jj + X$	558	491^{+0}_{-7}
$e^+e^-\, jj + X$	116	105^{+1}_{-5}

TABLE II: Summary of LO and NLO cross sections [pb] for $W/Z + 0, 1, 2$ jets, including single leptonic decay of the weak boson. The central value at NLO is for $\mu = M_V$, and the uncertainty at NLO is for scale variation from $\mu = M_V/2$ to $\mu = 2M_V$. No uncertainties are shown for LO results, as they are all considerably larger than at NLO. All Monte Carlo statistical uncertainties are less than 1%.

jet p_T distribution for the $W^\pm j$ and $W^\pm jj$ cases in Fig. 4, and for Zj and Zjj in Fig. 5. The leading order curves for $W^\pm + 1$ jet in Fig. 3 show a kinematic structure not present in the other curves. At leading order, the cut on the minimum p_T of a jet, Eq. (7) also imposes a minimum transverse momentum for the W boson, since at this order the transverse momenta are equal and opposite. Most events lie right above the cut, $p_T(W) \sim 20$ GeV. The vector addition of this peaked distribution with the transverse momentum generated in the decay leads to the structure shown in Fig. 3. At NLO (or for higher jet multiplicity), the jet transverse momentum cut does not impose the same constraint on the momentum of the W boson. This explains the absence of the structure in the other plots. The existence of this structure in the LO plots reinforces the importance of NLO calculations.

In contrast to the $W, Z + 1$ jet cases, the p_T distributions turn over at small values for $V + 2$ jets. If the highest p_T jet has a transverse momentum, $p_T^{(1)}$, close to 20 GeV, there is little phase space for the emission of a second, softer jet with $p_T^{(1)} > p_T^{(2)} > p_T^{min} = 20$ GeV.

We show the boson p_T distributions in Figs. 6,7, and the dijet invariant mass distributions in Figs. 8,9. The former show a pronounced NLO deficit relative to LO at large values of

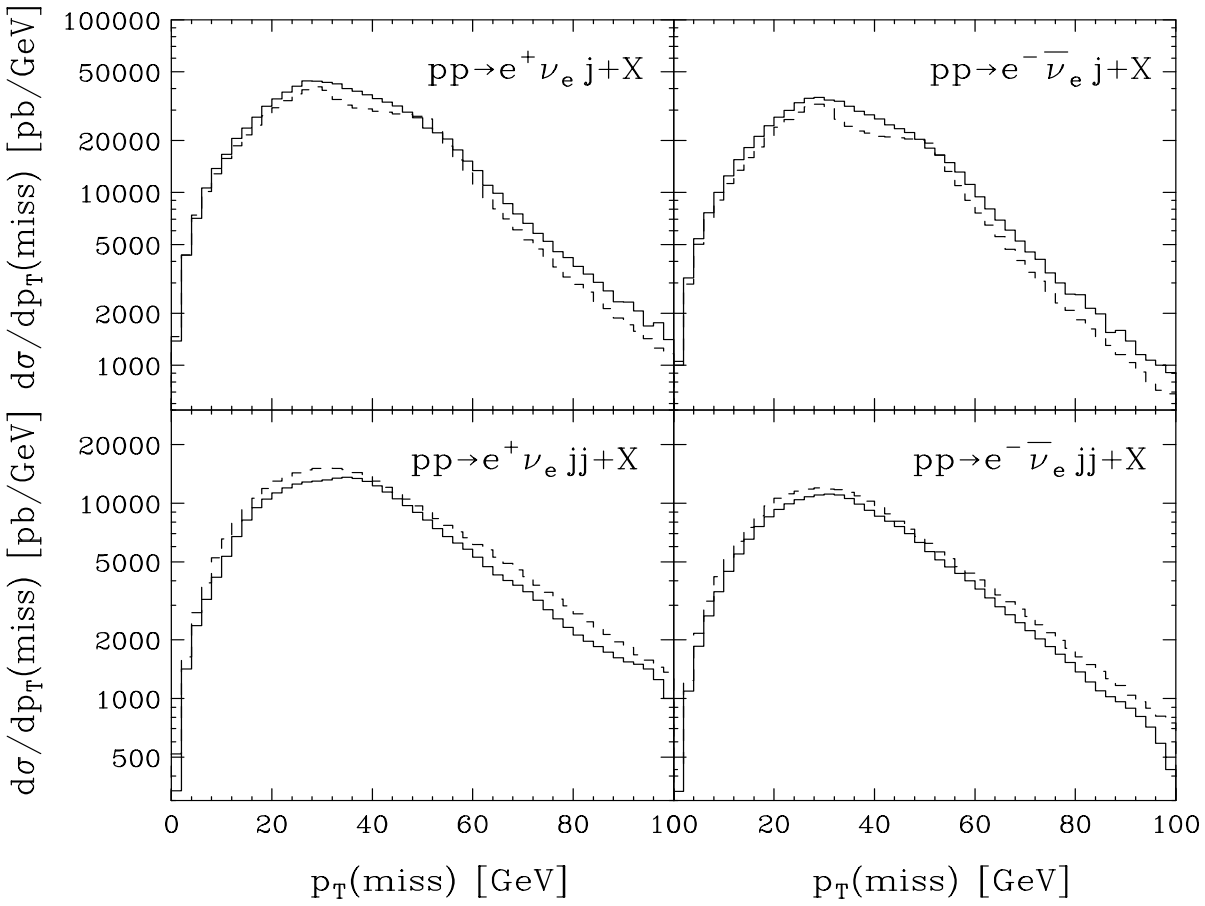

FIG. 3: The missing transverse momentum distribution of $e^{\pm}\nu_e\, j$ and $e^{\pm}\nu_e\, jj$ events at LO (dashed) and NLO (solid).

$p_T(V)$, whereas for the latter there is almost no change in shape from LO to NLO. The same holds true for the pseudo-rapidity separation of the jet pair, as shown in Figs. 10, 11.

III. HEAVY FLAVOR CONTENT OF JETS

We calculate the fraction of $W, Z+2$ jet events that contain two heavy quark jets, limiting ourselves to b quarks, because they can be tagged with high efficiency in experiment. These processes are of particular interest as backgrounds to new physics searches, in particular Higgs bosons. The calculations are identical to those presented in Ref. [1], but for pp collisions at the LHC energy of $\sqrt{s} = 14$ TeV. We work in the approximation in which the b quarks are taken to be massless, as the massive results are not yet known at NLO, and we ignore contributions from processes in which there are b quarks already present in the initial state.

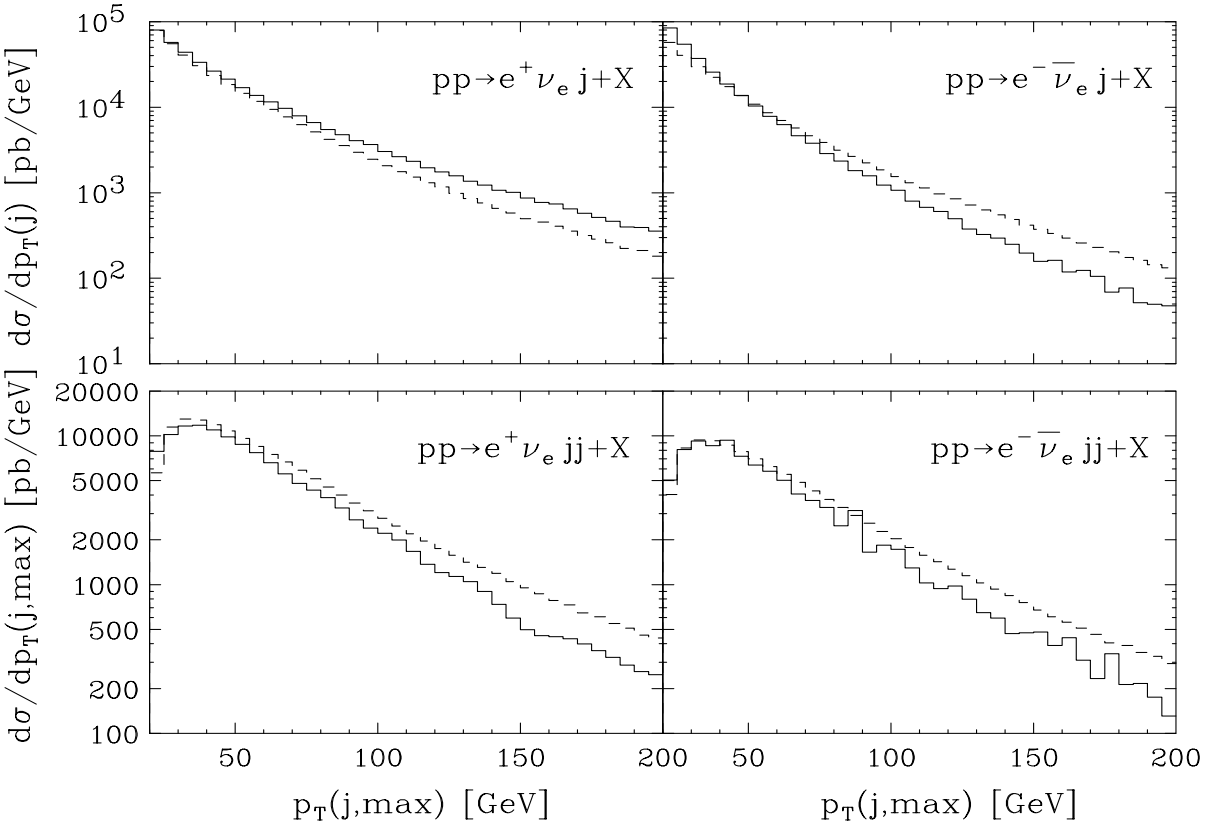

FIG. 4: Hardest jet p_T distribution of $e^{\pm}\nu_e\, j$ and $e^{\pm}\nu_e\, jj$ events at LO (dashed) and NLO (solid).

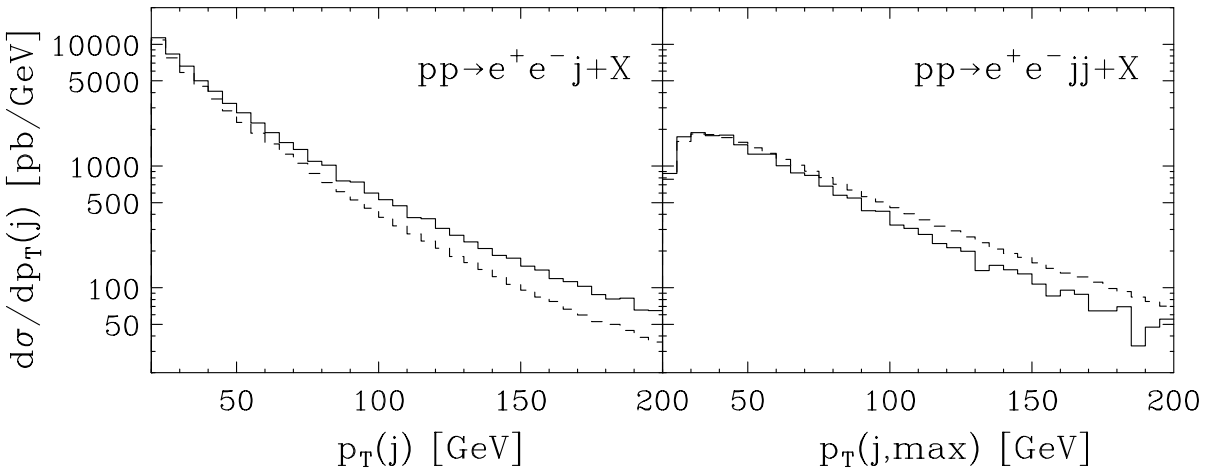

FIG. 5: Hardest jet p_T distribution in $e^+e^-\, j$ and $e^+e^-\, jj$ events at LO (dashed) and NLO (solid).

We begin as in the non-heavy flavor case, checking the theoretical uncertainty of the calculation by plotting the scale dependence of the cross sections, shown in Figs. 12,13. The $W + b\bar{b}$ cross section shows much greater μ dependence at NLO than at LO, contrary to naïve expectations. For the central scale choice $\mu = M_W$, the NLO result is a factor 2.4 larger than at LO, and requires some explanation. At LO, charge conservation allows only $q\bar{q}$ initial

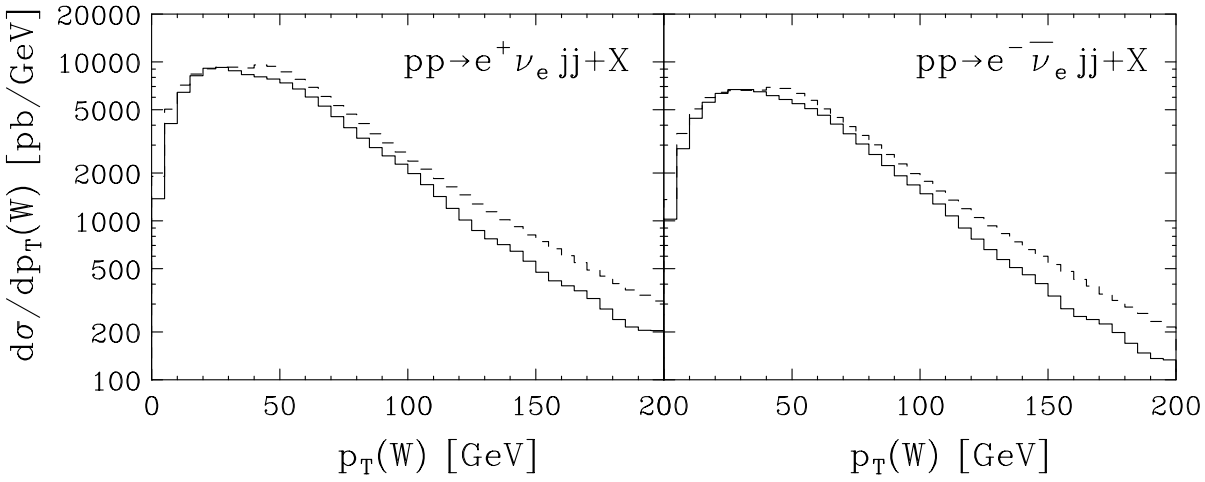

FIG. 6: The boson p_T distribution of $e^{\pm}\nu_e\, jj$ events at LO (dashed) and NLO (solid).

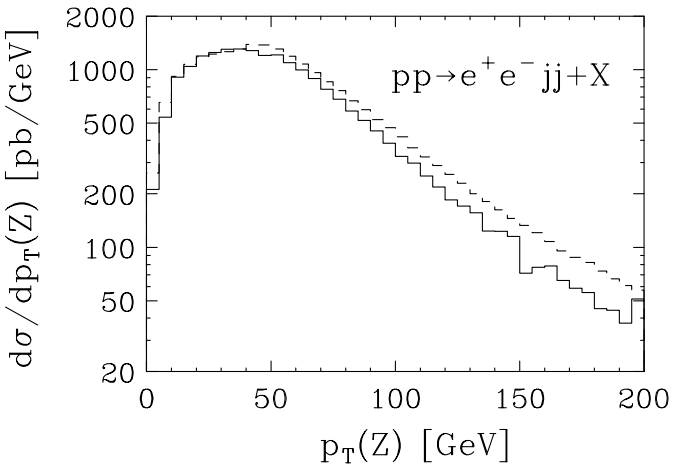

FIG. 7: The boson p_T distribution in $e^+e^-\, jj$ events at LO (dashed) and NLO (solid).

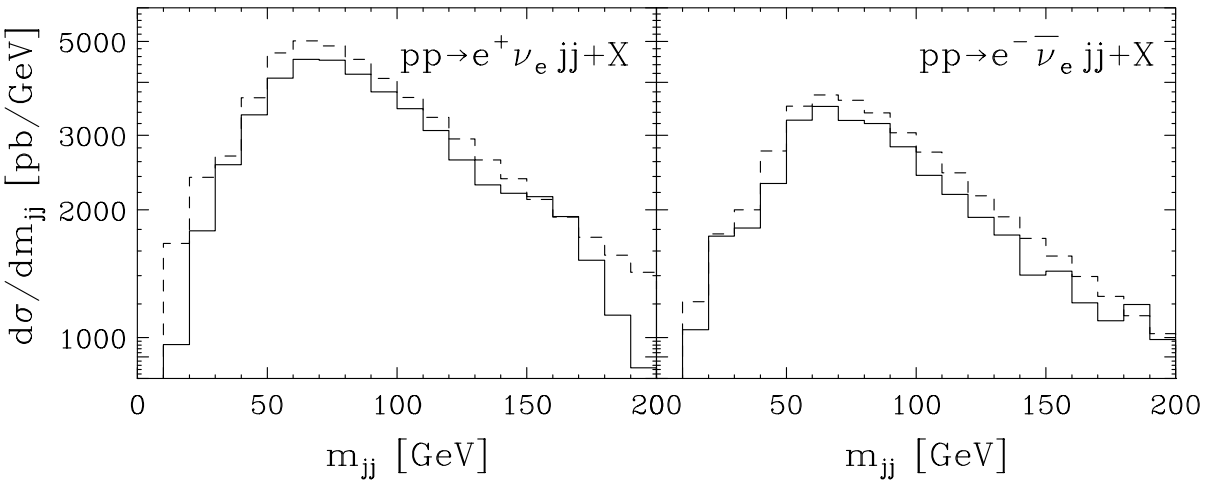

FIG. 8: The jet pair invariant mass distribution of $e^{\pm}\nu_e\, jj$ events at LO (dashed) and NLO (solid).

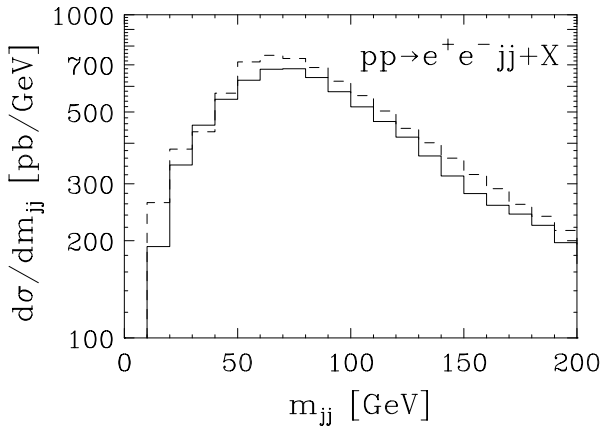

FIG. 9: The jet pair invariant mass distribution of $e^+e^-\,jj$ events at LO (dashed) and NLO (solid).

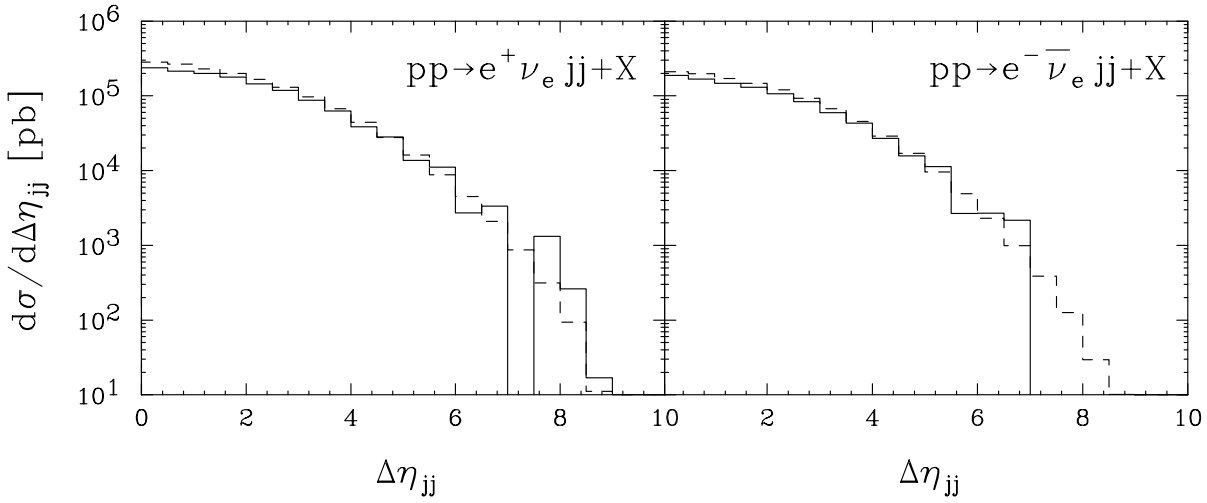

FIG. 10: The jet pair η separation distribution of $e^{\pm}\nu_e\,jj$ events at LO (dashed) and NLO (solid).

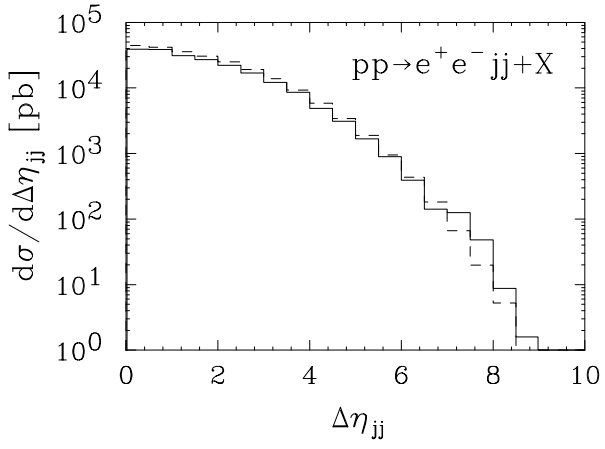

FIG. 11: The jet pair η separation distribution of $e^+e^-\,jj$ events at LO (dashed) and NLO (solid).

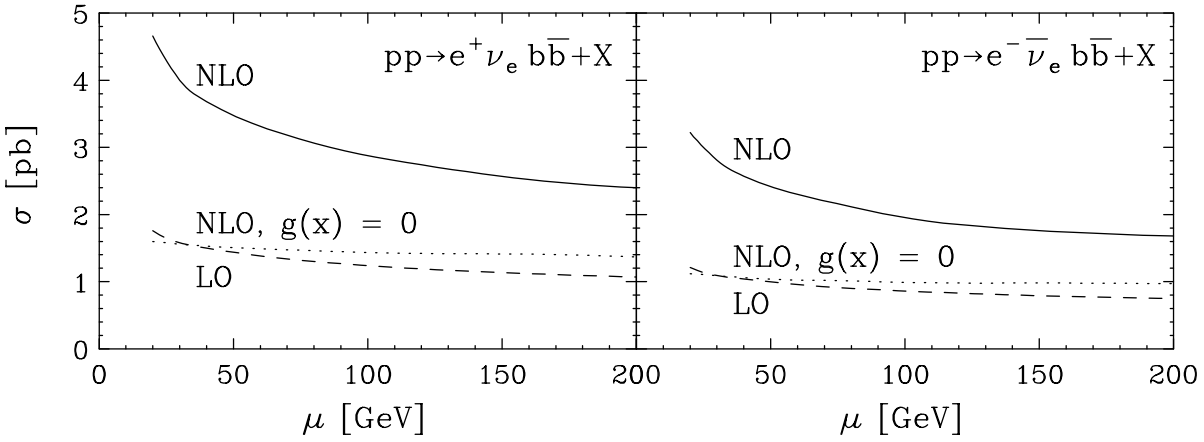

FIG. 12: Scale dependence of the $e^{\pm}\nu_e\, b\bar{b}$ cross sections, $\mu = \mu_r = \mu_f$, using the cuts described in Sec. II B. Note the behavior of $Wb\bar{b}$ at NLO: the NLO rate with initial gluon density set to zero is well-behaved, but with real initial gluons it behaves much more like a LO calculation. See text for additional comments.

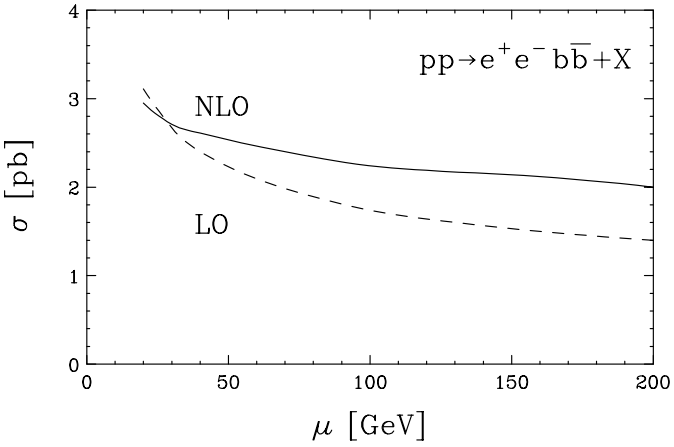

FIG. 13: Scale dependence of the $e^+e^-\, b\bar{b}$ cross section, $\mu = \mu_r = \mu_f$, using the cuts described in Sec. II B. The $Zb\bar{b}$ result is better behaved than in the case of $Wb\bar{b}$, but still retains an uncertainty of order $\pm 15\%$.

states to contribute to $Wb\bar{b}$ production. At NLO, the same is true for the virtual corrections, but not for the real emission corrections, which contain subprocesses $qg \to q'Wb\bar{b}$. Some representative Feynman diagrams are shown in Fig. 14. This allows the very large gluon luminosity at the LHC to contribute. However, if we ignore the additional $b\bar{b}$ pair, then NLO corrections are of Drell-Yan type, Fig. 14(a), and might be expected to receive an additional contribution of only 30% at LHC energies (see Table II). The remaining contribution is due to diagrams of the type shown in Figs. 14(b,c), which contain no singularities for a

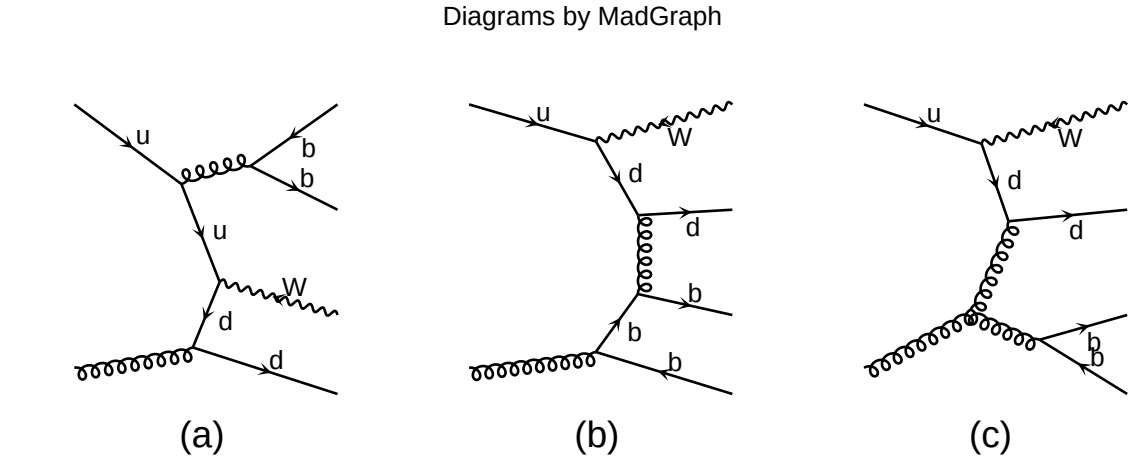

FIG. 14: Some representative diagrams for the process $ug \to dW^+b\bar{b}$. See text for discussion.

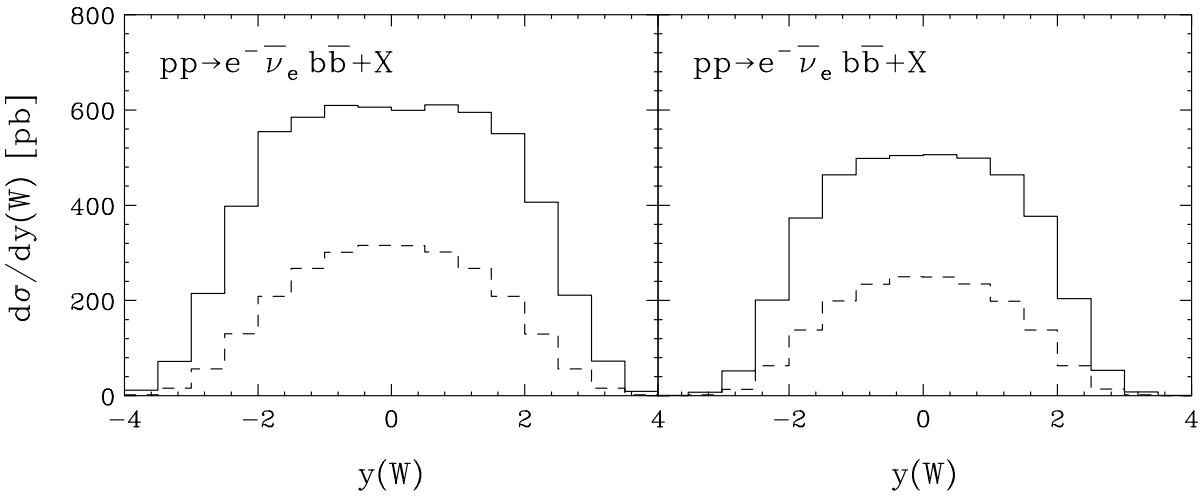

FIG. 15: The W rapidity distribution of $e^{\pm}\nu_e\, b\bar{b}$ events, at LO (dashed) and NLO (solid). The broad plateau which appears at NLO is indicative of the significant contribution from a qg-initiated component.

finite b mass; W emission requires the massless quark propagator to be off mass shell [17]. (We calculate with $m_b = 0$, but avoid the massless singularity by imposing a finite p_T cut on both b quarks.) The contributions from diagrams of the type in Fig. 14(b) open up additional phase space, since they are not suppressed by an s-channel gluon propagator which occurs in diagrams of the type shown in Fig. 14(a). Furthermore, contributions from diagrams of the type in Fig. 14(c) contain a large Casimir factor from the three-gluon vertex. Diagrams (b) and (c) constitute new, LO contributions that cannot appear in Drell-Yan. Note, however, that one cannot consider individual diagrams separately, as they must all be included together at the amplitude level to maintain gauge invariance. We demonstrate that

the additional diagrams are the cause of the hugely enhanced cross section by calculating the NLO $W^{\pm}b\bar{b}$ cross section with initial gluons turned off, *i.e.* $g(x) = 0$. This result has practically no μ dependence, as shown by the dotted curves in Fig. 12. This is further supported by examining the rapidity distribution of the emitted W boson, shown in Fig. 15. The significant NLO enhancement at large rapidity, resulting in a noticeable plateau in the distribution, demonstrates the large size of the qg-initiated component: quarks on average occur at larger values of Feynman x than gluons, resulting in an overall boost of the W boson in the rest frame of the detector. Thus, the dominant component of inclusive $W^{\pm}b\bar{b}$ production at LHC energies, the summed gluon-initiated real emission subprocesses, still contains large LO theoretical uncertainty. This can be resolved only by performing a NLO calculation of $W^{\pm}b\bar{b}j$.

This situation does not exist for $Zb\bar{b}$ production, because lack of a flavor-changing constraint on any quark line means that initial state gluons contribute already at LO. This is readily apparent from Fig. 13, which shows NLO corrections much closer to the size expected for Drell-Yan processes, and a residual uncertainty due to scale dependence of about 20%. Note the significant feature of the heavy flavor case, that $\sigma(W^+b\bar{b}) \gtrsim \sigma(Zb\bar{b}) \gtrsim \sigma(W^-b\bar{b})$, as opposed to $\sigma(W^+jj) \gtrsim \sigma(W^-jj) \gg \sigma(Zjj)$ for the flavor-inclusive cross sections.

As for the $W^{\pm}jj$ case in Sec. II D, we histogram the differential $W^{\pm}b\bar{b}$ cross sections as a function of the p_T of the leading jet, shown in Fig. 16, along with the desired ratios of $W^{\pm}jj$ to $W^{\pm}b\bar{b}$ cross sections, to illustrate the relative behavior of heavy flavor production. In principle, $W^{\pm}c\bar{c}$ production would behave similarly to $W^{\pm}b\bar{b}$. We also show the distributions as a function of dijet invariant mass in Fig. 17. Including the b quark mass at LO is only a 4% effect on the total cross section, but is contained almost completely in the invariant mass range $2m_b < m_{bb} < 20$ GeV. Consequently, the two m_{bb} curves would exactly overlap each other in Fig. 17, except in the first bin.

Similar histograms for the $Zb\bar{b}$ case are shown in Figs. 18,19. Table III summarizes the $W^{\pm}, Z + b\bar{b}$ cross section results and scale uncertainties.

IV. APPLICATIONS

One of the principle goals of the LHC program is to determine the nature of electroweak symmetry breaking (EWSB), which in the Standard Model (SM) is due to a complex scalar

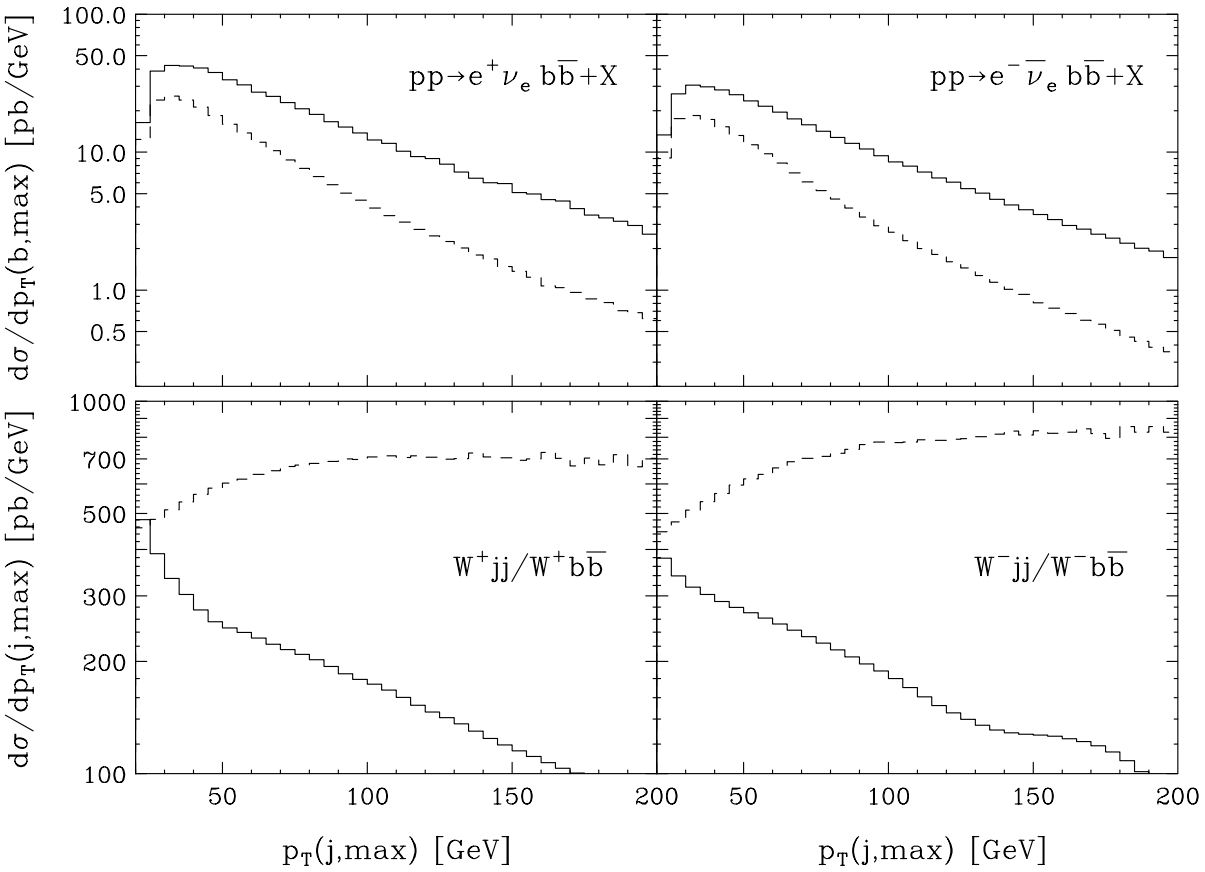

FIG. 16: The leading jet p_T distribution of $e^{\pm}\nu_e\, b\bar{b}$ events, and of the ratio of $W^{\pm}\, jj$ to $W^{\pm}\, b\bar{b}$, at LO (dashed) and NLO (solid). For the latter, the jets from $W^{\pm}\, jj$ are also restricted to the region $|y_j| < 2.5$, to match the acceptance cuts that will be used for $W^{\pm}\, b\bar{b}$ events.

process	σ_{LO}	σ_{NLO}
$e^+\nu_e\, b\bar{b} + X$	$1.30^{+0.21}_{-0.18}$	$3.06^{+0.62}_{-0.54}$
$e^-\nu_e\, b\bar{b} + X$	$0.90^{+0.14}_{-0.12}$	$2.11^{+0.46}_{-0.37}$
$e^+e^-\, b\bar{b} + X$	$1.80^{+0.60}_{-0.40}$	$2.28^{+0.32}_{-0.29}$

TABLE III: Summary of LO and NLO cross sections [pb], including the theoretical (scale) uncertainty at NLO, for $W/Z + b\bar{b}$, including leptonic decay of the weak boson. The central value at NLO is for $\mu = M_V$. All Monte Carlo statistical uncertainties are less than 1%.

$SU(2)$ doublet field. Upon acquiring a vacuum expectation value, it gives rise to both weak boson and SM fermion masses and creates a single physical scalar, the Higgs boson. While there are other variations on this idea, or other models which generate EWSB, nearly

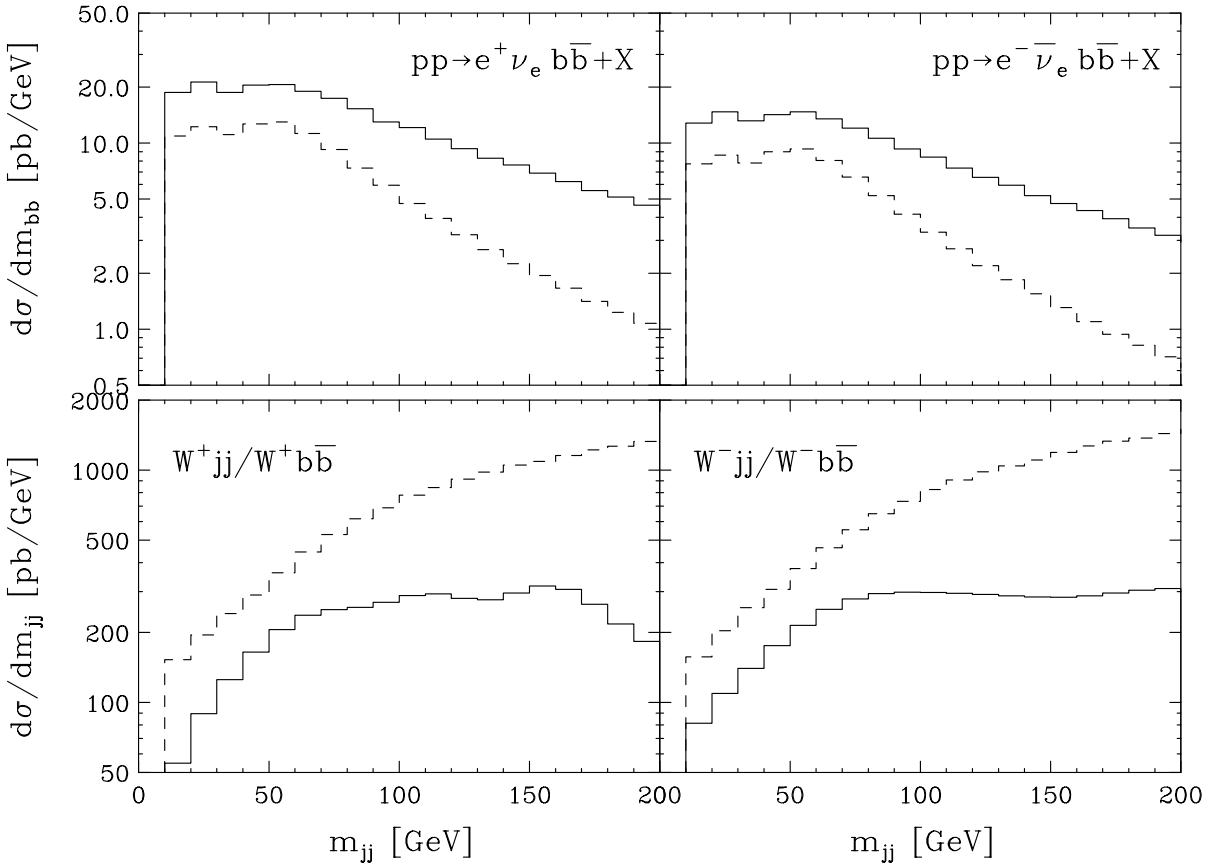

FIG. 17: The dijet invariant mass distribution of $e^{\pm}\nu_e\, b\bar{b}$ events, and of the ratio of $W^{\pm}\, jj$ to $W^{\pm}\, b\bar{b}$, at LO (dashed) and NLO (solid). For the latter, the jets from $W^{\pm}\, jj$ are also restricted to the region $|y_j| < 2.5$, to match the acceptance cuts that will be used for $W^{\pm}\, b\bar{b}$ events.

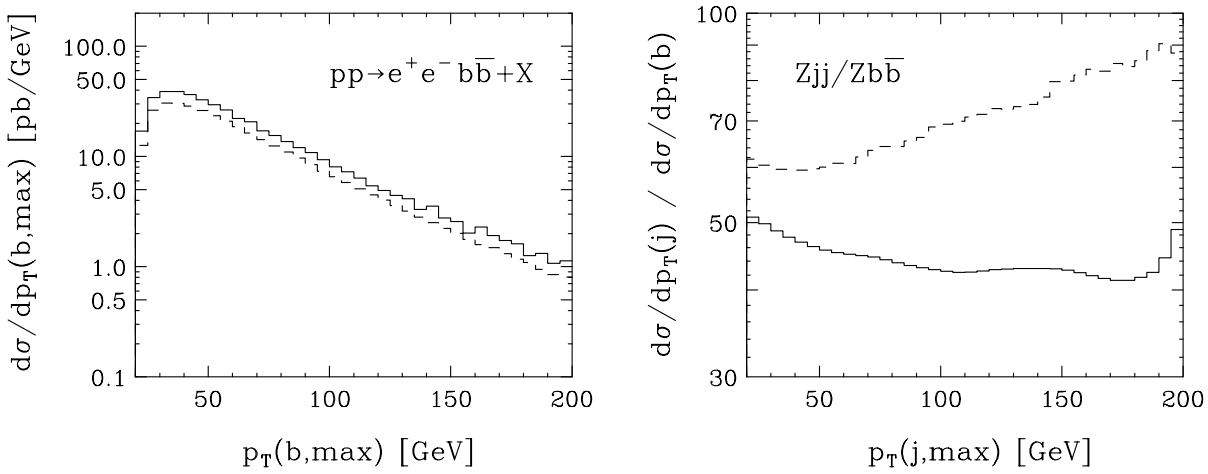

FIG. 18: The leading jet p_T distribution of $e^+e^-\, b\bar{b}$ events,and of the ratio of Zjj to $Zb\bar{b}$, at LO (dashed) and NLO (solid). For the latter, the jets from Zjj are also restricted to the region $|y_j| < 2.5$, to match the acceptance cuts that will be used for $Zb\bar{b}$ events.

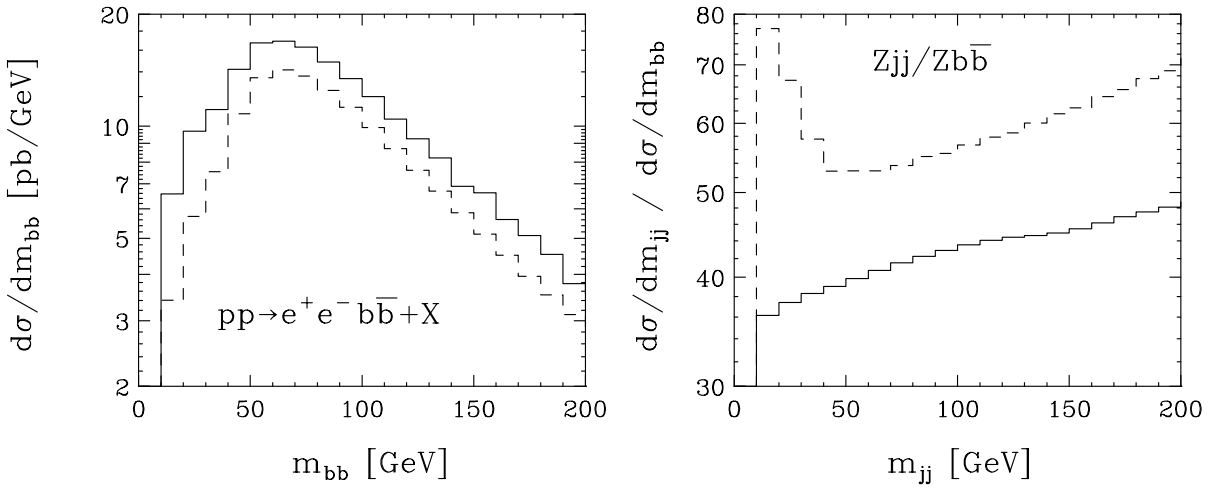

FIG. 19: The dijet invariant mass distribution of $e^+e^-\,b\bar{b}$ events, and of the ratio of Zjj to $Zb\bar{b}$, at LO (dashed) and NLO (solid). For the latter, the jets from Zjj are also restricted to the region $|y_j| < 2.5$, to match the acceptance cuts that will be used for $Zb\bar{b}$ events.

all of them have a physical scalar field which couples to weak bosons and SM fermions similar to the SM Higgs boson. Many searches for it at hadron colliders look for associated Higgs boson production, $pp \to W^{\pm}H, ZH$ [19], or a Higgs boson produced between two far forward/backward high-p_T jets. The latter is weak boson fusion (WBF) Higgs boson production, which arises from a pair of initial-state quarks both emitting either a W^+W^- or ZZ pair, which fuse to create the Higgs boson [20].

Precise theoretical knowledge of the $W, Z+$ jets cross sections is of particular interest at the LHC, since these processes constitute significant backgrounds for the above Higgs boson searches, as well as other SM processes of interest, such as top quark production, and many other new physics searches. We choose to examine only two particular cases: $W^{\pm}b\bar{b}$ as a background to $W^{\pm}H; H \to b\bar{b}$, and Zjj as a background to WBF Higgs production, $pp \to Hjj$.

A. $W^{\pm}b\bar{b}$ and $W^{\pm}H; H \to b\bar{b}$

The most desirable Higgs boson search channels at the LHC are inclusive production ($gg \to H$ via a top quark loop) or WBF Higgs production, due to their much larger cross section and much cleaner background environment, respectively. Despite the smaller rate, the $W^{\pm}H; H \to b\bar{b}$ channel has generated great interest because of its potential to measure

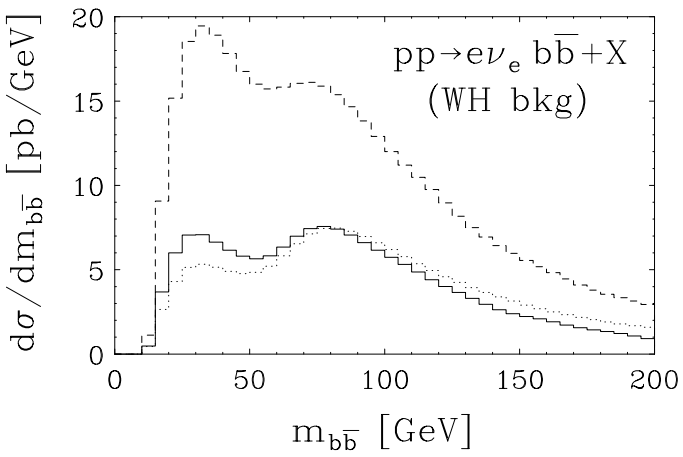

FIG. 20: The $b\bar{b}$ invariant mass distribution of $e^{\pm}\nu_e b\bar{b}$ events at LO (dotted), NLO (dashed), and NLO with a jet veto on the non-b real emission (solid), with kinematic cuts specific to a potential $W^{\pm}H; H \to b\bar{b}$ search as described in the text.

the bottom quark Yukawa coupling. Several LHC experimental groups [21, 22] have studied the channel in detail. These studies claim that the search will be quite difficult for Higgs boson masses above the current LEP limits, but possible. While the signal is known at NLO, our calculation of the $W^{\pm}b\bar{b}$ background at NLO is the first to rectify this omission.

As shown in Sec. III, the NLO cross section is more than two times the LO result. This does not bode well for this particular Higgs boson search channel. However, we must apply the same kinematic cuts as in the current analyses and examine the NLO/LO ratio in a dijet invariant mass bin relevant for the search. We apply the following cuts as in Ref. [21]:

$$p_T(\ell) > 20 \text{ GeV} , \quad |y_\ell| < 2.4 , \tag{10}$$

$$p_T(j) > 30 \text{ GeV} , \quad |y_j| < 2.5 , \tag{11}$$

$$\triangle R_{j\ell} > 0.4 , \quad \triangle R_{\ell\ell} > 0.2 , \tag{12}$$

where the jet may or may not be a b jet. The resulting $b\bar{b}$ invariant mass distribution is shown for the summed W^+ and W^- components in Fig. 20. Assuming a Higgs boson mass of $M_H = 120$ GeV, and a mass bin of ± 20 GeV, *i.e.* $100 < m_{jj} < 140$ GeV, the NLO cross section is a factor 1.9 larger than LO.

Since we know that the component causing the large enhancement typically has an additional jet emission at large p_T, we impose a non-b jet veto at NLO in the real emission calculation. This turns the cross section into an exclusive result, where the heavy flavor is assumed to have been tagged. This NLO exclusive result is about 10% smaller than the LO

result, making the background much more manageable. *However*, we emphasize that use of this result requires normalizing a parton shower calculation to this cross section *after* a light-jet veto is imposed in the parton shower Monte Carlo! The residual uncertainty from scale variation is $\approx^{+44}_{-70}$ %.

B. Zjj and Hjj

A characteristic feature of WBF Higgs boson production is Hjj events with the Higgs boson appearing at central rapidities, but the two scattered quarks appearing at large rapidities with significant p_T. Because the process is color singlet exchange, the events typically have little central jet emission. In contrast, QCD Zjj production prefers the jets to be much more central, while the Z comes from Bremsstrahlung and is at larger rapidites. Also, the color triplet or octet exchange gives rise to significant additional central jet emission, known as "minijet" activity [23, 24]. We use MCFM here to provide a NLO normalization of the QCD Zjj rate in a region of phase space relevant for WBF Higgs boson searches where the Higgs boson decays to tau pairs.

Standard kinematic cuts for these searches will require the jets, frequently called "tagging jets", to have a minimum separation of about 4 units of pseudo-rapidity, to appear in opposite hemispheres, and for the Higgs decay products (*e.g.* $\tau^+\tau^-$) to appear between the jets [25]. In addition to the basic cuts of Eqs. (6-8), we thus impose the following cuts:

$$|\eta_j^{(1)} - \eta_j^{(2)}| > 4.0 \ , \qquad \eta_j^{(1)} \cdot \eta_j^{(2)} < 0 \ , \qquad \eta_j^{min} + 0.4 < \eta_{\ell_1,\ell_2} < \eta_j^{max} - 0.4 \ , \tag{13}$$

where η_j^{max} (η_j^{min}) is the larger (smaller) of $\{\eta_j^{(1)}, \eta_j^{(2)}\}$. This reduces the QCD Zjj cross section from 94.9 pb to 2.9 pb at LO, and 104 pb to 3.4 pb at NLO. Comparison to previous experimental studies are difficult, as all of these used dynamical scales, and were all different from each other [26].

We show the scale dependence for $Z + 2$ jets in this phase space configuration in Fig. 21. The NLO is quite stable, as in the total cross section result, except for very low values of μ. This is not uncommon in NLO calculations and typically indicates the presence of logarithms that can become large with small choices of μ, but are not necessarily a problem at that order in the perturbative expansion. We also plot several differential distributions in Fig. 22 to demonstrate that there do not appear to be any large NLO corrections to the shapes in

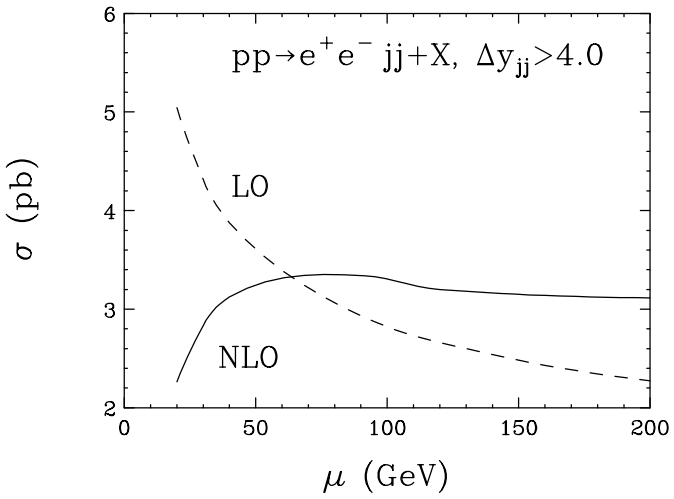

FIG. 21: Scale dependence of the e^+e^-jj ($\tau^+\tau^-jj$) cross section, $\mu = \mu_r = \mu_f$, using the cuts described in Sec. IV B to examine the region of far forward tagging jets.

this small region of phase space; the NLO distributions in general appear to be very similar to the LO distributions. One notable exception is the azimuthal angle between the tagging jets, which is flatter at NLO, compared to the preferential back-to-back configuration of the jets at LO. This is likely due to emission of final state radiation spreading out the preference for the QCD jet pair to be back-to-back, but requires further investigation. This distribution is of special relevance for studies of Higgs CP transformation properties [27].

V. CONCLUSIONS

We have presented the first results for the implementation of $W/Z + 2$ jet production at NLO at the LHC, including the specific cases of heavy flavor jets. An analysis based on inclusive jet production for the LHC shows that in most cases the usual benefits of NLO are realized, among them a reduced scale dependence and hence an improved normalization for kinematic distributions. The outstanding exception is the case of $W^{\pm}b\bar{b}$ production, which at one higher order in the QCD coupling experiences additional LO contributions that dramatically enhance the total rate. We showed that this additional contribution typically leads to an additional non-b jet at large p_T and pseudo-rapidity, which can be identified in the detectors.

These processes are of particular interest at the LHC as backgrounds to other SM processes and searches for new physics. We analyzed two cases in particular. The first analysis,

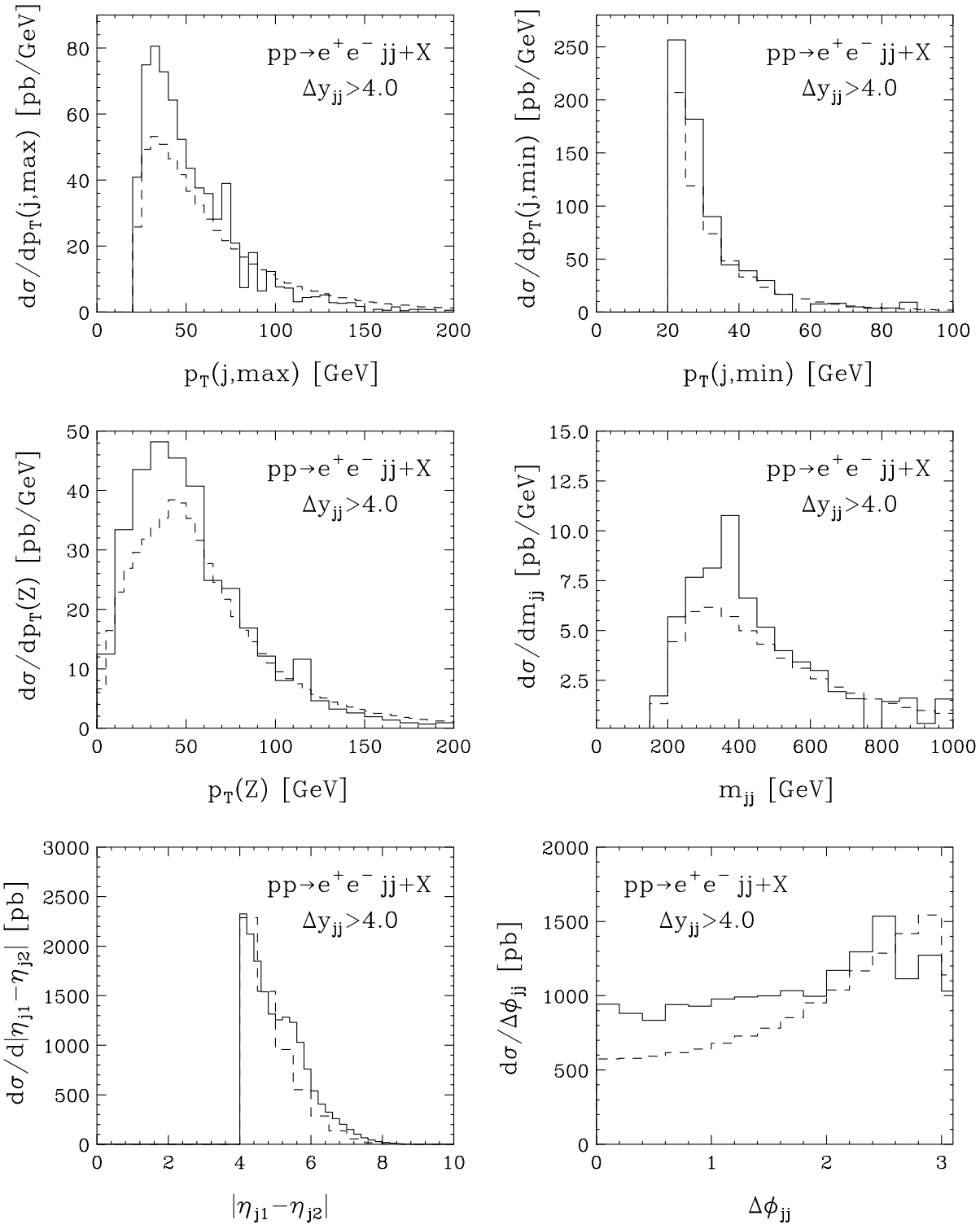

FIG. 22: Various kinematic distributions for QCD e^+e^-jj ($\tau^+\tau^-jj$) production as a background to Hjj production, as described in the text.

$W^{\pm}b\bar{b}$ as a background to $WH; H \to b\bar{b}$ for a light Higgs boson, suffers considerably from the unexpected large NLO corrections, but may be controlled somewhat by vetoing non-b jets. This will require additional analysis with parton shower Monte Carlo normalized to our NLO jet-vetoed rates, after the veto of additional jets radiated in the parton shower. The second analysis, Zjj as a background to weak boson fusion Higgs production, Hjj, shows that the overall corrections are not very large for a central scale choice of $\mu = M_Z$, only about $+14\%$. However, most Hjj analyses have used dynamical scale choices of $p_T(j, min)$, which average only a few tens of GeV, so these analyses will generally benefit from a reduction in the QCD Zjj background normalization. In addition, we have shown that no large NLO corrections appear in this tiny region of phase space with jets widely separated in pseudo-rapidity, and various kinematic differential distributions at NLO appear very much like their LO counterparts. This allows simple overall normalization of parton shower Monte Carlo based on the total rates, but does not address the issue of vetoing events with additional minijet activity.

Acknowledgments

This work was supported in part by the U.S. Department of Energy under Contracts No. W-31-109-ENG-38 (Argonne) and No. DE-AC02-76CH03000 (Fermilab). We would like to thank Volker Drollinger, Tilman Plehn and Dieter Zeppenfeld for useful discussions.

---

[1] J. Campbell and R. K. Ellis, Phys. Rev. D **65**, 113007 (2002).

[2] Z. Bern, L. J. Dixon and D. A. Kosower, Nucl. Phys. B **513**, 3 (1998).

[3] Z. Nagy and Z. Trocsanyi, Phys. Rev. D **59**, 014020 (1999) [Erratum-ibid. D **62**, 099902 (1999)].

[4] F. A. Berends, W. T. Giele and H. Kuijf, Nucl. Phys. B **321**, 39 (1989).

[5] K. Hagiwara and D. Zeppenfeld, Nucl. Phys. B **313**, 560 (1989).

[6] R. K. Ellis, D. A. Ross and A. E. Terrano, Nucl. Phys. B **178**, 421 (1981).

[7] S. Catani and M. H. Seymour, Nucl. Phys. B **485**, 291 (1997) [Erratum-ibid. B **510**, 503 (1997)].

[8] W. T. Giele, E. W. Glover and D. A. Kosower, Nucl. Phys. B **403**, 633 (1993).

[9] R. Hamberg, W. L. van Neerven and T. Matsuura, Nucl. Phys. B **359**, 343 (1991) [Erratum-ibid. B **644**, 403 (2002)].

[10] R. K. Ellis and S. Veseli, Phys. Rev. D **60** (1999) 011501.

[11] J. M. Campbell and R. K. Ellis, Phys. Rev. D **62**, 114012 (2000).

[12] H. Georgi, Nucl. Phys. B **363**, 301 (1991).

[13] J. Pumplin *et al.*, JHEP **0207**, 012 (2002).

[14] G. C. Blazey *et al.*, arXiv:hep-ex/0005012.

[15] P. B. Arnold and M. H. Reno, Nucl. Phys. B **319**, 37 (1989) [Erratum-ibid. B **330**, 284 (1989)].

[16] P. Arnold, R. K. Ellis and M. H. Reno, Phys. Rev. D **40**, 912 (1989).

[17] A check using MADEVENT [18], which shows the approximate relative weighting of each graph's contribution, did not reveal any emphasis of t-channel gluon contributions.

[18] F. Maltoni and T. Stelzer, JHEP **0302**, 027 (2003).

[19] S. L. Glashow, D. V. Nanopoulos and A. Yildiz, Phys. Rev. D **18** (1978) 1724; J. F. Gunion, P. Kalyniak, M. Soldate and P. Galison, Phys. Rev. Lett. **54**, 1226 (1985); ibid., Phys. Rev. D **34**, 101 (1986); A. Stange, W. J. Marciano and S. Willenbrock, Phys. Rev. D **49**, 1354 (1994); ibid., Phys. Rev. D **50**, 4491 (1994).

[20] D. A. Dicus and S. S. Willenbrock, Phys. Rev. D **32**, 1642 (1985).

[21] V. Drollinger, T. Muller and D. Denegri, arXiv:hep-ph/0201249.

[22] B. P. Kersevan and E. Richter-Was, Eur. Phys. J. C **25**, 379 (2002); ATLAS Collaboration, ATLAS TDR, Ch. 15, CERN/LHCC/99-15.

[23] V. D. Barger, R. J. Phillips and D. Zeppenfeld, Phys. Lett. B **346**, 106 (1995).

[24] D. Rainwater, R. Szalapski and D. Zeppenfeld, Phys. Rev. D **54**, 6680 (1996).

[25] D. Rainwater, D. Zeppenfeld and K. Hagiwara, Phys. Rev. D **59**, 014037 (1999).

[26] S. Asai *et al.*, ATL-PHYS-2003-005; G. Azuelos and R. Mazini, ATL-PHYS-2003-004.

[27] T. Plehn, D. Rainwater and D. Zeppenfeld, Phys. Rev. Lett. **88**, 051801 (2002).